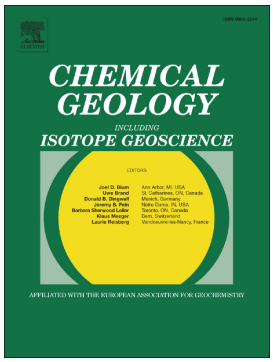

The lithium and magnesium isotope signature of olivine dissolution in soil experiments

Philip A.E. Pogge von Strandmann, Phil Renforth, A. Joshua West, Melissa J. Murphy, Tu-Han Luu, Gideon M. Henderson

PII: S0009-2541(20)30547-7

DOI: https://doi.org/10.1016/j.chemgeo.2020.120008

Reference: CHEMGE 120008

To appear in: *Chemical Geology*

Received date: 28 May 2020

Revised date: 11 November 2020

Accepted date: 26 November 2020

Please cite this article as: P.A.E. Pogge von Strandmann, P. Renforth, A.J. West, et al., The lithium and magnesium isotope signature of olivine dissolution in soil experiments, *Chemical Geology* (2020), https://doi.org/10.1016/j.chemgeo.2020.120008

The lithium and magnesium isotope signature of olivine dissolution in soil experiments

Philip A.E. Pogge von Strandmann[1,2,*] ppoggevo@uni-mainz.de; Phil Renforth[3]; A. Joshua West[4]; Melissa J. Murphy[2]; Tu-Han Luu[5]; Gideon M. Henderson[6]

[1]Institute of Geosciences, Johannes Gutenberg University, 55122 Mainz, Germany.

[2]Institute of Earth and Planetary Sciences, University College London and Birkbeck, University of London, Gower Street, London WC1E 6BT, UK.

[3]Research Centre for Carbon Solutions, School of Engineering and Physical Sciences, Heriot-Watt University, Edinburgh, EH14 4AS, UK.

[4]Department of Earth Sciences, University of Southern California, 3651 Trousdale Parkway – ZHS 117, Los Angeles, CA 90089, USA

[5]Bristol Isotope Group, Bristol University, Wills Memorial Building, Queen's Road, Bristol, BS8 1RJ, UK.

[6]Department of Earth Sciences, Oxford University, South Parks Road, Oxford, OX1 3AN, UK.

[*]Corresponding author.

Abstract

This study presents lithium and magnesium isotope ratios of soils and their drainage waters from a well-characterised weathering experiment with two soil cores, one with olivine added to the surface layer, and the other a control core. The experimental design mimics olivine addition to soils for CO_2 sequestration and/or crop fertilisation, as well as natural surface addition of reactive minerals such as during volcanic deposition. More generally, this study

presents an opportunity to better understand how isotopic fractionation records weathering processes. At the start of the experiment, waters draining both cores have similar Mg isotope composition to the soil exchangeable pool. The composition in the two cores evolve in different directions as olivine dissolution progresses. Mass balance calculations show that the water δ^{26}Mg value is controlled by congruent dissolution of carbonate and silicates (the latter in the olivine core only), plus an isotopically fractionated exchangeable pool. For Li, waters exiting the base of the cores initially have the same isotope composition, but then diverge as olivine dissolution progresses. For both Mg and Li, the transport down-core is significantly retarded and fractionated by exchange with the exchangeable pool. This observation has implications for the monitoring of enhanced weathering using trace elements or isotopes, because dissolution rates and fluxes will be underestimated during the time when the exchangeable pool evolves towards a new equilibrium.

Keywords: Chemical weathering; lithium; magnesium; stable isotopes; weathering rate; soil core experiments

1. Introduction

Chemical weathering of continental silicate rocks supplies alkalinity and cations that drive carbonate formation and provides nutrients to the ocean to fuel primary productivity and organic carbon burial (Berner, 2003; Ebelmen, 1845). Because these are the primary processes removing CO_2 from the atmosphere on timescales >10^5 years, weathering is a key process driving climate change over geologic time (Berner et al., 1983; Colbourn et al., 2015;

Godderis et al., 2013). A climate-driven feedback may make silicate weathering a dominant climate-moderating process, helping to explain the long-term stability of Earth's climate (Walker et al., 1981). However, the strength of this feedback is disputed, in part because supply of weatherable material (high activity primary silicates) also exerts an important control on weathering fluxes (Goudie and Viles, 2012; Pogge von Strandmann et al., 2017a; Pogge von Strandmann et al., 2017c; Raymo et al., 1988; West et al., 2005).

Despite considerable research, the fundamental processes controlling weathering, and ultimately the evolution of atmospheric pCO_2, are still poorly known. Understanding the relative roles of climate vs. material supply in determining weathering fluxes is challenging because the weathering mechanisms that operate at soil profile scales remain difficult to resolve. Moreover, it has proven difficult to relate soil-scale processes to those that operate at catchment and global scales, given the heterogeneities in supply of fresh primary rock, mineral saturation, pH, mineral surface area, reactivity and temperature in natural environments (e.g., Gislason et al., 2009; Maher and Chamberlain, 2014; Stallard and Edmond, 1983; Stefansson and Gislason, 2001; West et al., 2005). Laboratory experiments provide insight into mineral weathering rates and their dependence on many of these parameters, but rates calculated from laboratory experiments are generally several orders of magnitude higher than those observed in natural environments (White and Brantley, 2003), suggesting that the underlying mechanisms may also differ. To address this discrepancy, experiments emulating the inherently complex processes operating in the natural environment are necessary.

The uncertainty in understanding weathering rates in natural systems has further implications for understanding the potential for "enhanced weathering" as a strategy for removing anthropogenic CO_2 from the atmosphere (Andrews and Taylor, 2019; Schuiling and Krijgsman, 2006; Taylor et al., 2020). Proposals for enhanced weathering include spreading finely-ground silicate and carbonate minerals on land surfaces (Hartmann et al., 2013; Koehler et al., 2010; Renforth, 2012; Schuiling and Krijgsman, 2006), in coastal environments (Hangx and Spiers, 2009; Schuiling and de Boer, 2010), and in the ocean (Koehler et al., 2013; Renforth et al., 2013). In each case, the aim is to increase the amount of mineral dissolution and associated CO_2 drawdown. However, without precise knowledge of weathering rates, it is not yet possible to determine whether enhanced weathering would be a net sink of CO_2, given the energy required for rock grinding and transportation (Moosdorf et al., 2014; Renforth, 2012).

A relatively new development in the study of weathering is the use of "non-traditional" stable isotopes. A number of these systems are fractionated by weathering processes and therefore have the potential to trace weathering, and even determine weathering fluxes. These tools could offer significant advantages over approaches that require several simultaneous measurements (e.g. multiple elemental concentrations, runoff rates, surface area, etc.). Magnesium isotopes ($\delta^{26}Mg$) are such a potential tracer of weathering processes, useful because Mg is a direct part of the long-term carbon cycle (Berner et al., 1983). Magnesium is present in both silicate and carbonate rocks, and these components typically have significantly different isotope ratios (Huang et al., 2013; Li et al., 2010; Saenger and Wang, 2014). This difference means that the $\delta^{26}Mg$ of rivers is controlled both by lithology and by additional, smaller fractionation during

uptake of mostly heavy Mg during formation of secondary minerals (Liu et al., 2014; Opfergelt et al., 2014; Opfergelt et al., 2012; Pogge von Strandmann et al., 2008; Pogge von Strandmann et al., 2012; Ryu et al., 2016; Tipper et al., 2010; Tipper et al., 2008; Tipper et al., 2006b; Wimpenny et al., 2011; Wimpenny et al., 2014).

Lithium isotopes (δ^7Li) also show promise as an isotopic tracer of weathering, unusual in being dominantly controlled by silicate weathering. The Li isotope ratio is unaffected by plant uptake and primary productivity (Lemarchand et al., 2010; Pogge von Strandmann et al., 2016), and negligibly influenced by weathering of carbonates, even in carbonate-dominated catchments (Kisakürek et al., 2005; Millot et al., 2010; Pogge von Strandmann et al., 2017b). The δ^7Li of silicate rocks comprises a narrow range ($\delta^7Li_{continental\ crust}$ ~ 0.6 ± 0.6‰ (Sauzéat et al., 2015), δ^7Li_{basalt} ~ 3–5‰ (Elliott et al., 2006)) relative to that in rivers (2–43‰, global mean ~23‰ (Dellinger et al., 2015; Huh et al., 1998; Murphy et al., 2019; Pogge von Strandmann et al., 2006)). The high variability in rivers is caused by preferential uptake of ^{6}Li into secondary minerals formed during weathering, driving residual waters isotopically heavy (Huh et al., 2001; Huh et al., 1998; Kisakürek et al., 2005; Lemarchand et al., 2010; Liu et al., 2015; Millot et al., 2010; Pistiner and Henderson, 2003; Pogge von Strandmann et al., 2010; Pogge von Strandmann et al., 2006; Pogge von Strandmann and Henderson, 2015; Pogge von Strandmann et al., 2014; Vigier et al., 2009; Wimpenny et al., 2015; Wimpenny et al., 2010). Dissolved Li isotope ratios are therefore controlled by the ratio of primary mineral dissolution (supplying low, rock-like, δ^7Li to solution), relative to secondary mineral formation (preferentially removing ^{6}Li and therefore leading to high dissolved

δ^7Li). This balance means that dissolved Li isotopes trace what is often referred to as the congruency of silicate weathering (where congruent weathering features a high ratio of primary mineral dissolution to secondary mineral formation) (Bouchez et al., 2013; Dellinger et al., 2015; Misra and Froelich, 2012; Pogge von Strandmann et al., 2010; Pogge von Strandmann and Henderson, 2015).

In this study, we examine Mg and Li isotope ratios from a well-characterised soil weathering experiment (Renforth et al., 2015). The aims of this study are (i) to better understand the processes that affect dissolved Li and Mg isotope compositions, (ii) to assess whether these isotopic tracers are useful for determining weathering processes and rates, including in enhanced weathering applications, and (iii) to compare isotopic methods with a more conventional approach to calculating weathering rates using elemental concentrations and ratios (Renforth et al., 2015).

2. Experimental approach

As a step towards bringing the inherently complex weathering environment into controlled laboratory conditions, 1 m long soil cores were taken from agricultural land. These cores are described in detail in Renforth et al., 2015. Briefly, three cores were extracted from the same location, in North Oxfordshire, UK. The bedrock in the region is Jurassic limestone and mudstone, and the soils are generally calcareous. The cores span the ploughed layer (~10cm), the underlying B and C horizons, and parent rock material at the bottom of the cores. One core was used to examine the bulk soil composition. The other two were used as column reactors, with a modified Hoagland nutrient

solution (~200 μg g^{-1} K, N, 30 μg g^{-1} P, 37 ng g^{-1} Ca, 30 ng g^{-1} S; 0.2ng g^{-1} Li, 69 ng g^{-1} Mg,) dripped into the top of each soil column at 15 ml h^{-1} for 133 days at a constant temperature of 19°C. The Hoagland solution was used to mimic the effect of fertiliser added to an agricultural setting. The observed residence time of water in each column was approximately 3 days (observed as the continuing drip time once influent water was shut off), similar to the residence time expected based on the flow rate and measured porosity, of 3.3 days. The influent solution was mixed in four separate, but identical, sequential batches. Effluent waters exited the base of each column continuously and were sampled periodically for chemical analysis. Effluent pH exhibited no trends with time (7.5 ± 0.2 for the control core and 7.2 ± 0.2 for the olivine core (Renforth et al., 2015)). To minimise evaporative loss, source beakers, collection beakers, and the soil columns were capped, with solution removed or introduced via tubing. Water samples were collected periodically from the base of each soil column.

To mimic weathering of fresh silicate, 100 g of crushed olivine was stirred into the top of one of the cores ("olivine core") at the start of the 133-day experiment, while nothing was added to the control core, although the top was also stirred (Fig. 1). The olivine grain size was determined by dry sieving (78% had a particle diameter of >125μm; for full grain size characterisation see Renforth et al., 2015). The olivine grain surface area was measured by BET, giving 3.04 ± 0.03 m^2 g^{-1}. Our experimental approach, of sudden addition of a mineral to the soil surface, mimics other sudden-addition scenarios, such as deposition of volcanic ash deposits or intentional mineral addition to consume CO_2 by enhanced weathering.

The study of Renforth et al. (2015) determined the dissolution rate of the ground olivine added to soils, based on effluent major element concentrations such as Mg and Si. That study also determined a mineral surface-area-dependent weathering rate for such "enhanced" experiments.

3. Methods

Major element concentrations in bulk soils and olivine powder were determined by XRF (Renforth et al., 2015). For isotope separation, material was dissolved in concentrated HF-HNO_3-$HClO_4$ at elevated temperature in PFA beakers on hotplates, followed by evaporation to dryness and sequential heated re-dissolution first in concentrated HNO_3 and then in 6M HCl. Exchangeable and carbonate fractions were also sampled using a sequential extraction technique (Tessier et al., 1979): the exchangeable fraction was extracted with 1M Na acetate (pH 8.2), while the carbonate fraction was dissolved with Na acetate buffered to pH5 with acetic acid. The effluent solutions collected from the bottom of the soil columns were passed through 0.2 μm membrane Whatmann cellulose nitrate filters before analysis (Renforth et al., 2015).

For Mg isotopes, ~0.4–1μg of Mg was purified through a two-stage cation exchange procedure (Pogge von Strandmann et al., 2011; Pogge von Strandmann et al., 2019c) and analysed relative to the standard DSM-3 on a Thermo Neptune MC-ICP-MS at the Bristol Isotope Group (Pogge von Strandmann et al., 2012). Seawater and BCR-2 were also analysed following identical purification procedures, giving long-term (during 10 years of analyses) values of $\delta^{26}Mg$ = -0.83 ± 0.05‰ (n = 33; chemistry = 27, where "chemistry" refers to standards processed through full procedural chemistry as used for samples, and

uncertainty is 2sd) and -0.25 ± 0.05‰ (n = 18; chemistry = 16), respectively, in keeping with other studies, as reported in prior compilations (Foster et al., 2010; Pogge von Strandmann et al., 2011; Shalev et al., 2018; Teng et al., 2015).

For Li isotope analysis, sufficient drip water was evaporated to attain 20ng of Li. Lithium was separated using a two-stage cation exchange technique, described in detail elsewhere (Pogge von Strandmann and Henderson, 2015), and analysed on a Nu Instruments HR MC-ICP-MS (high resolution multi-collector inductively coupled plasma mass spectrometer) at Oxford University. Results are given as ‰ deviation from the standard L-SVEC. To assess accuracy and precision, seawater and USGS standards BCR-2 (basalt) and SGR-1 (shale) were analysed, giving δ^7Li = 31.3 ± 0.6‰ (n = 50, chemistry = 50), 2.7 ± 0.4‰ (n = 4, chemistry = 4) and 3.6 ± 0.4‰ (n = 3, chemistry = 3), respectively, which are in agreement with other studies (Dellinger et al., 2015; Phan et al., 2016; Pogge von Strandmann et al., 2019a; Pogge von Strandmann et al., 2012).

4. Results

4.1 Mg isotopes

The MgO content of the olivine was 47.7 wt%, with a δ^{26}Mg of -0.23 ± 0.06 ‰, identical to mantle-derived olivine (Pogge von Strandmann et al., 2011). In contrast, the bulk soils had around 0.50 ± 0.03 wt% MgO and a δ^{26}Mg of -0.44‰ (Table 1). Around 0.5% of the initial bulk soil Mg was in the exchangeable fraction, based on the Na-acetate leach. Exchangeable Mg was isotopically light (-1.54 to -2.48‰; Fig. 2B). The carbonate fraction (comprising ~16% of the total soil Mg) was isotopically even lighter (δ^{26}Mg = -3.24 to -3.31‰), in the range of previously measured carbonate rocks (~-4 to -1‰) (Saenger and Wang, 2014;

Tipper et al., 2006b). Residual soils (i.e. after removal of exchangeable and carbonate fractions), accounting for the remaining ~84% of total Mg (likely contained in clay minerals), had δ^{26}Mg values indistinguishable from those of the initial bulk soil. Towards the base of the soil column, bulk soil had δ^{26}Mg values similar to primary silicates (~-0.2‰), which likely made up the initial composition of the silicate portion of the soil.

Magnesium was not deliberately added to the influent solution, although a background concentration of 69 ng ml^{-1} was measured. The drip waters from the control column started at ~7 μg ml^{-1} Mg and gradually decreased to 4.5 μg ml^{-1} over time (Fig. 3C; Table 2). Effluent-water concentrations from the olivine core were between 1 and 5 μg g^{-1} higher. The decrease in overall Mg concentrations with time in effluent waters from both cores is discussed in Renforth et al. (2015) and is attributed to carbonate and exchangeable complexes adjusting to the composition of the artificial drip waters (e.g., adjustment of the exchangeable complex to a different influent composition compared to natural rain experienced in the field). Renforth et al. (2015) used the difference in [Mg] between the olivine treatment and the control to derive olivine dissolution rates. The drip water δ^{26}Mg from both columns started at approximately the same value (-2‰), and the two solutions became resolvably distinct from each other after ~17 days. The waters from the control core then became isotopically lighter almost linearly with time, with a final value of -2.73‰ (Fig. 3D). In contrast, the olivine core drip waters were almost unchanged over time, resulting in a difference between the two columns ($\Delta^{26}Mg_{olivine\text{-}control}$) of 1‰ by the end of the experiment.

4.2 Li isotopes

The Li concentration of the olivine was 1.2 μg g^{-1}, with a δ^7Li of 2.7 ± 0.3‰, identical to the mantle (Lai et al., 2015; Marschall et al., 2017). The Li concentration of the bulk soils was fairly low (1–3 μg g^{-1}) compared to the upper continental crust (30.5 ± 3.6 μg g^{-1}) or silicate-rich soils (1.1–130 μg g^{-1}) (Lemarchand et al., 2010; Pogge von Strandmann et al., 2012; Sauzéat et al., 2015). The δ^7Li of the soils ranged between -0.7 and 2.1‰ (Fig. 2A; Table 1), largely within the reported range for the continental crust (0.6 ± 0.6‰) (Sauzéat et al., 2015).

Approximately 0.5% (0.2–0.7%) of bulk soil Li was in the exchangeable fraction (Na acetate leach – Table 1), similar to Mg. The δ^7Li of this exchangeable fraction varied between -5.9 and +6.6‰ (Fig. 2A). The Li concentrations in the carbonate leach were below detection limits (<0.01 ng/g); thus ≈99.5% of the Li was in silicate fractions.

The Li concentration in the effluent drip waters was 1.1 ± 0.3 ng g^{-1} in the control column and 1.3 ± 0.2 ng g^{-1} in the olivine column (Fig. 3A; Table 2). A total of ~9.6 μg Li was added to the columns from the original input solution during the entire experiment, representing 16–18% of the concentration in the effluent solutions. The δ^7Li of the influent water was 12.3 ± 0.4‰. In comparison, the mass of Li in the control column's exchangeable fraction (see below for calculation) was ~57 μg Li, six times more than the added Li.

The effluent δ^7Li started out in both cores at similar values (~13‰). The effluent water composition stayed at approximately 12‰ in both cores for the first ~20 days of the experiment (Fig. 3B), after which the control core waters

increased to a maximum of 24.2‰ by 54 days, and then remained relatively constant. In contrast, the olivine core effluent's δ^7Li was lower and did not increase beyond 16.6‰, resulting in a difference between the two columns ($\Delta^7Li_{olivine\text{-}control}$) of -7 to -10‰ by the end of the experiment.

4.3 Mass balance

A mass balance of elemental influx and output can be constructed, based on several assumptions. The first is that the input-corrected effluent flux of Ca from the control column is solely due to the dissolution of carbonates within the core. This was shown by Renforth et al. (2015) who report a linear correlation between [Ca] and total inorganic carbon in the bulk solid-phase of the cores. We also assume that the input-corrected effluent flux of Si from the control column is due to dissolution of silicates (clays, given a lack of primary silicates) within the core. We use the measured x/Ca and x/Si (where x is either Mg or Li) ratios of the leached and residual silicate and carbonate fractions to determine the mass of Mg and Li in the core and in particular, the proportion that each phase contributes to the material exiting the core in the effluent solutions. We assume that all effluent Li and Mg that remains after correcting for input, silicate and carbonate dissolution stems from the soil's exchangeable fraction:

$$X_{exch} = X_{influent} - X_{effluent} - X_{silicate} - X_{carbonate} \quad \text{Eqn. 1}$$

$$X_{exch} = X_{influent} - X_{effluent} - \left[\left(\frac{X}{Si}\right)_{clay} \times Si\right] - \left[\left(\frac{X}{Ca}\right)_{carb} \times Ca\right] \quad \text{Eqn. 2}$$

where X is the flux (in μg) of Li or Mg; 'Si' and 'Ca' are the fluxes of Si and Mg; exch, clay and carb are the exchangeable, clay and carbonate fraction, respectively. Then, based on the assumption that the cores are identical, we can

further determine the amount of Li and Mg that stems from the dissolution of olivine in the olivine core:

$$X_{exch} = X_{influent} - X_{effluent} - X_{silicate} - X_{carbonate} - X_{olivine} \quad \text{Eqn. 3}$$

We emphasise that this mass balance calculation is not determining the partitioning of Mg or Li between the different solid phases within the soil, but between the contributors of Mg and Li to effluent solution. The uncertainties of this mass balance stem from analytical uncertainty on the concentration measurements, which then propagate, so that the larger mass balance contributors (e.g. carbonate for Mg) have a larger influence on the ultimate error. Error propagation of the analytical uncertainties yield ±~6% relative error on the mass balance.

5. Discussion

5.1 Elemental mass balances

5.1.1 Magnesium

The mass balance of the effluent from the control core after 5 days from the start of the experiments shows that ~55% of the Mg stems from carbonate dissolution and ~42% from the exchangeable fraction (so these two sources make up >97% of the total eluted Mg) (Fig. 4). Less than 0.5% is initially from the dissolution of clay. By the end of the experiment, over 4 months later, the proportion from carbonate dissolution has increased to 65% at the expense of the contribution from the exchangeable fraction (Fig. 4).

In the olivine column, after 5 days from the start of the experiment olivine dissolution contributes ~19% of the dissolved Mg. By the end of the experiment,

olivine is the largest supplier of Mg (~45%), greater than Mg from carbonates or the exchangeable fraction (Fig. 4).

5.1.2 Lithium

The lithium mass balance of the effluent from the control core after 5 days is dominated by Li from the exchangeable pool (>84%), while clay only contributes ~1.5% and carbonates 0.05% (with the remaining ~14% coming from Li in the initial input solution). The fractions of Li from each source remain largely unchanged during the course of the experiment (~85% from the exchangeable fraction by the end) (Fig 5).

In the olivine core, after 5 days only 5% of the effluent's Li is sourced from olivine dissolution, while by the end of the experiment ~10% is from the olivine, with the remainder still dominated by exchangeable Li. The lack of Li in the soil carbonates motivates the use of Li as a silicate weathering tracer, independent of carbonate sources (Gou et al., 2019; Kisakürek et al., 2005), but also shows that in these soil solutions both primary and secondary silicates provide less Li than the exchangeable pool. The results also show that Mg and Li can be decoupled during weathering, even though Li substitutes for Mg in both primary and secondary silicates (Hindshaw et al., 2019).

5.2 Magnesium isotopes

5.2.1 Mg isotopes in the soils

The selective leaches of the different phases at different depths of the soil show that the carbonates are isotopically light (~-3.3‰), the silicates are isotopically heavy (~0‰), and the exchangeable fraction has an intermediate

composition (~-1.8‰), as also observed by other soil and carbonate studies (Chapela Lara et al., 2017; Opfergelt et al., 2014; Saenger and Wang, 2014; Tipper et al., 2006b). There is comparatively little isotopic variation with depth in any of the phases (Fig 2), although the δ^{26}Mg of the exchangeable fraction increases by ~0.6‰ with depth.

5.2.2 Control core behaviour during the experiment

For the first 17 days of the experiment, the δ^{26}Mg of the control core's effluent solution stayed approximately constant (and similar to that of the olivine core, discussed below). The significant effect on the Mg mass balance of the exchangeable fraction (42%) suggests that the initial effluent must be strongly affected by the composition and nature of this fraction. It is likely that ion exchange retarded the downward transport of the Mg added to the influent solution, while the change in solution chemistry led to release of previously adsorbed Mg. If, as is likely, the [Mg] in the influent solutions was not in equilibrium with the exchangeable pool (because the [Mg] is likely lower than that in the original pore waters, as well as potentially due to changes in pH, temperature, etc.), Mg was released from the exchangeable pool, and the Mg concentration of the effluent solution decreased with time (Fig. 3C), resulting in a decrease in the proportion of exchangeable Mg provided to solution with time (Fig. 4). Thus, because of the retardation by ion exchange, the duration of the downward movement in the core of Mg is not three days (the water residence time), but around 17 days, a feature discussed further in the context of Li isotopes below.

Following this initial period of time, the δ^{26}Mg of the control core's effluent solution started to decrease almost linearly to a final value of -2.73‰ (Fig. 3D), without reaching any obvious isotopic steady-state. The mass balance shows that this decrease is largely due to increasing contribution from the dissolution of (isotopically light) carbonates with time.

Based on a standard isotopic mass balance equation (identical in assumptions to that described in Section 4.3) it is possible to calculate the isotope ratio of Mg coming from the exchangeable pool at the start of the experiment.

$$\delta_{effluent} = (f\delta)_{influent} + (f\delta)_{exch} + (f\delta)_{sil} + (f\delta)_{carb} \qquad \text{Eqn. 4}$$

where f is the Mg mass fraction each phase makes up of the total, and δ is the isotope ratio. The calculated isotopic composition can then be compared to the isotope ratio of the leached exchangeable fraction, and any difference will be due to fractionation caused by isotopic exchange. We find that the δ^{26}Mg exiting the exchangeable pool is approximately -1‰, exhibiting a fractionation factor of ~0.56‰ from the lowest exchangeable fraction. This amount of isotope fractionation is similar to that reported from exchange experiments (Wimpenny et al., 2014) and observed in soil profiles (Tipper et al., 2010) and basaltic groundwaters (Oelkers et al., 2019), suggesting that, while most of the Mg is sourced from carbonate dissolution (65% by the end of the experiment), the observed isotope ratio in the effluent is due to mixing between light Mg from the carbonate and fractionated Mg from the exchangeable pool (which contributes ~32% of Mg).

5.2.3. Olivine core behaviour

As described above, the $\delta^{26}Mg$ of the control and the olivine core were identical for the first 17 days of the experiment, due to retardation of the Mg signal by ion exchange as fluids travelled down the soil column. Once the chemical signal of added (fractionated) Mg reached the bottom of the core, $\delta^{26}Mg$ in the effluent from the olivine core increased relative to that from the control core (Fig. 3), and by the end of the experiment was ~1‰ higher than that of the control core. The elemental mass balance shows that this increase was due to addition of isotopically heavy Mg from olivine dissolution.

The impact of olivine dissolution vs. the combination of carbonate and exchangeable Mg is demonstrated by plotting $\delta^{26}Mg$ as a function of Mg/Ca ratios (Fig. 6). The olivine core clearly has higher Mg/Ca ratios and higher $\delta^{26}Mg$ values, indicating addition of high-Mg, isotopically heavy material — as expected for olivine.

Renforth et al. (2015) derived an olivine dissolution rate for these core experiments by comparing the Mg flux from both cores. Here, we observe a significant ($p < 0.05$) relationship between $\Delta^{26}Mg_{olivine\text{-}control}$ (i.e., the difference between the two cores that reflects the specific effect of olivine dissolution on the dissolved Mg isotope composition) and the olivine dissolution rate calculated from Mg fluxes (Renforth et al., 2015) (Fig. 8B). Although there is some scatter (largely because $\Delta^{26}Mg$ increases linearly with time, while Δ[Mg] does not), the amount of isotopic difference between the effluent of the two cores increases both with time and with the olivine dissolution rate. This is to be expected if the only tangible difference between the two cores is the dissolution of the added (isotopically heavy) olivine. However, we note that the absolute amount and rates of dissolving olivine inferred both from the mass balance and from the

isotope ratios are likely lower than the true values, due to retardation by the exchangeable pool, and hence olivine-derived Mg taking longer than expected to exit the core to be analysed.

From an overall weathering perspective, the data from these core experiments indicate that lithology (i.e. silicates vs. carbonates) exerts a significant control on Mg isotopes, in agreement with other studies (Li et al., 2010; Pogge von Strandmann et al., 2019b; Teng et al., 2010; Tipper et al., 2008; Tipper et al., 2006a; Tipper et al., 2006b). Retardation by ion exchange provides an additional element of complication: on long, natural weathering, timescales, Mg isotopes appear to be a useful tracer of weathering lithology, and potentially also silicate weathering characteristics. However, on the timescales of this experiment, and indeed any weathering or enhanced weathering experiment where results are necessary within a relatively short period, ion exchange may mean that observed effects in drainage solutions do not necessarily reflect the total dissolution reactions taking place.

5.3 Lithium isotopes

5.3.1 Soil characteristics

The bulk rock δ^7Li values in the soil core are fairly constant with depth (-0.7 to +2.1‰). Studies on the δ^7Li of bulk soils in different settings show everything from little variation with depth (Huh et al., 2004; Lemarchand et al., 2010; Pistiner and Henderson, 2003), isotope ratios becoming lighter with depth (Clergue et al., 2015; Huh et al., 2004; Liu et al., 2013; Tsai et al., 2014) and isotope ratios becoming heavier with depth (Kisakurek et al., 2004; Liu et al., 2013; Pogge von Strandmann et al., 2012). Explanations for this behaviour range

from mixing of detrital material (e.g. Tsai et al., 2014) to fractionation during formation of secondary minerals and depletion of Li during weathering (e.g. Clergue et al., 2015). Here, the largely invariant δ^7Li values with depth suggest that, in terms of the silicates that control the bulk soil Li composition, there is little depth-variation in this profile.

To our knowledge, no study has yet examined how the exchangeable pool behaves in a soil profile, but broadly similar processes likely apply. In our first such profile, exchangeable δ^7Li reaches a peak of 12.6‰ at 30cm depth and then decreases to -6‰ at 80cm depth (Fig. 2). For most of the profile, the exchangeable pool is isotopically heavier than the bulk soil.

Overall, the exchangeable pool will have been exchanging Li with pore waters, with an isotope fractionation on the order of 10–20‰ towards lighter values (Pogge von Strandmann et al., 2019a; Hindshaw et al., 2019), as also calculated by mass balance below. This process should theoretically drive both pore waters and the exchangeable pool isotopically heavy with time (and depth). While this process appears to be occurring down to 30cm, below this depth the exchangeable pool becomes increasingly lighter and less concentrated, resulting in a positive co-variation between δ^7Li and [Li] in the exchangeable pool (Fig. 7). The reason for this trend is not entirely clear: a low Li concentration likely also reflects a low [Li] in the pore waters, which would then be expected to have a higher δ^7Li composition as material is removed and fractionated (Clergue et al., 2015; Pogge von Strandmann et al., 2017b), imparting high δ^7Li to the exchangeable pool. It is possible that exchange is slower deeper in the profile, as the proportion of primary carbonates increase, but the data do not allow us to definitively identify the mechanism.

While the exchangeable fraction only makes up ~0.5% of the Li in the bulk soil, and is therefore not important for the bulk soil δ^7Li composition, it has a considerably larger influence on the Li composition of the effluent solutions (Fig. 5).

5.3.2 Control core behaviour

As described in Section 5.1, the behaviour of effluent Li in the control core is entirely dominated by Li from the exchangeable pool (84.1% at the start of the experiment, and 84.7% by the end of the experiment).

The control and olivine cores exhibit identical δ^7Li behaviour for the first ~20 days (as opposed for ~17 days for Mg) of the experiment with a δ^7Li value of ~12‰ (Fig. 3B). Given the exchangeable fraction's dominance, the initial effluent's δ^7Li should be directly related to the δ^7Li of the exchangeable fraction at the bottom of the soil core. The solution composition is ~18‰ higher than the deepest exchangeable fraction, generally higher than previously reported fractionation during sorption of Li onto secondary minerals of 0–12‰, while structural Li tends to have fractionation factors >21‰ (Hindshaw et al., 2019; Millot and Girard, 2007; Pistiner and Henderson, 2003; Pogge von Strandmann et al., 2019a; Pogge von Strandmann et al., 2020). It may therefore be the case that the final fractionation is not only occurring between the deepest exchangeable fraction, but also layers further up the soil column with higher δ^7Li. The concentration-weighted average of the exchangeable fraction in the entire soil column is ~8‰, giving a fractionation factor of ~4‰, within the reported range for exchangeable Li. Alternatively or in addition, the isotopic composition may be

influenced by incorporation of Li into structural sites, with higher fractionation factors.

During the experiment, the control core's effluent δ^7Li increases rapidly to 20‰ and eventually stabilises at ~23‰. There is no evidence that the secondary mineralogy changed during this time, based on broadly constant mineral saturation states (kaolinite SI = 6.5 ± 0.6 (Renforth et al., 2015)). Instead, this behaviour is likely due to retardation by ion exchange (Davidson and Dickson, 1986; Johnson and DePaolo, 1997; Krishnaswami et al., 1982; Porcelli and Swarzenski, 2003), as the newly added dissolved Li moves down the core, similar to that observed for Mg. The [Li] in the influent solution is out of equilibrium with the exchangeable fraction (due to differences in composition, pH, temperature from the natural soil waters), so it liberates Li from the exchangeable pool. In other words, the change in δ^7Li after 20 days is due to the addition of influent material affecting the exchangeable pool. A similar isotopic mass balance as described above for Mg shows that the δ^7Li of material coming from the exchangeable pool is ~12.7‰, hence exhibiting a fractionation factor of ~18‰ from the lowest exchangeable fraction (similar to that inferred from the initial solutions). This heavy Li moves down the core, but because of retardation, the duration of this movement is not three days (the water residence time), but the observed ~20 days. This also means that the effluent isotope ratio will continue to evolve, as the lighter isotopes retained in the exchangeable fraction eventually also moves down the core and into the effluent. The retardation factor R for Li in the exchangeable fraction, assuming perhaps over-simplistically, a linear form of the Langmuir isotherm, is:

$$R = 1 + \frac{q}{C}$$ Eqn. 5

where q is the adsorbed ions and C the ions in effluent solution. This yields an R value of 1.85 for the final experimental sample for Li. In comparison, the R value for Mg is 1.32. Using a seepage velocity of 0.31 m/day (Fig. 1), this gives an exchangeable Li transport rate of 0.17 m/day for Li and 0.23 m/day for Mg. Theoretically, this means that it would take ~19 days for the heavy Li and ~14 days for the Mg to make it into the effluent solution. This is slightly shorter than the observed breakthrough time, but we note that the time resolution of the sampling is low, and the above calculations are based on constant Darcy velocities and porosities through the core. Importantly, the different retardation factors for Li and Mg explain why the apparent breakthrough times are different for the two elements. Such behaviour will further decouple Li and Mg isotopes.

The sorption partition coefficient can also be calculated from the retardation factor, according to (Krishnaswami et al., 1982):

$$K = \frac{q}{C}$$ Eqn. 6

where K is a dimensionless distribution coefficient. This is related to the 'normal' partition coefficient K_d by the equation:

$$K = K_d \left(\frac{\rho(1-n)}{n}\right)$$ Eqn. 7

By this calculation, the sorption partition coefficient is ~0.093 for Li, and ~0.037 for Mg. In other words, in this setting, Li sorbs ~2.6 times more readily than Mg, explaining the slightly longer retardation time for Li.

5.3.3 Olivine core behaviour

As described above, thed7Li of the effluent from the olivine core diverges from that of the control core beginning after ~20 days, ending up 7‰ lower (Fig. 3B). The retardation of the downward-flowing added Li (with associated isotopic fractionation) by the exchangeable pool functions identically in both the control and olivine core. However, in the olivine core, the addition of heavy Li from the exchangeable fraction is to an extent counterbalanced by addition of light Li from dissolution of the olivine (δ^7Li = 2.7‰).

The initial isotope fractionation between soil and effluent, or between olivine and effluent (average soil and olivine having virtually identical δ^7Li: 2.3 vs. 2.7‰, respectively), was $\Delta^7Li_{soil\text{-}solution}$ = ~-10‰ at the start of the experiment. After 20 days, the effluent from the olivine core has a δ^7Li value that increases, leading to $\Delta^7Li_{soil\text{-}solution}$ = -14‰ by the end of the experiment, compared to -21‰ in the control core (Fig. 3B). This difference suggests that olivine dissolution is not promoting relatively greater Li uptake by the exchangeable pool or by secondary minerals, which would drive δ^7Li higher than the control core. This amount of fractionation can be compared with the dissolution-precipitation batch-reactor olivine experiments conducted by Wimpenny et al. (2010a). A similar degree of isotopic fractionation between the initial olivine and final solution is observed in both experiments, even though Wimpenny et al. (2010a) did not conduct their experiments in soil. They concluded that this fractionation was due to chrysotile ($Mg_3(Si_2O_5)(OH)_4$) precipitation. In our study's soil experiments, however, chrysotile is always significantly undersaturated (average saturation index ~ -9), and instead the exchangeable pool appears to dominate Li behaviour.

The $\Delta^7Li_{olivine\text{-}control}$ values correlate with the olivine weathering rate calculated from the difference in Mg flux between the two cores (Renforth et al., 2015) (Fig. 8A; $r^2 = 0.72$). This correlation is consistent with a first-order control on the dissolved δ^7Li from primary mineral dissolution rates; that is to say, the more olivine dissolves, the more it contributes relatively unfractionated δ^7Li, thus decreasing the solution δ^7Li relative to the control core. The observed correlation is also consistent with an identical amount of adsorption (or secondary mineral formation) in both cores, meaning that the only additional control on the olivine core's effluent δ^7Li is olivine dissolution.

The core experiments also provide a test of the generally accepted controls on Li isotopes. The prevailing model is that dissolved Li isotopes are determined by weathering congruency, which is the ratio of primary mineral dissolution to secondary mineral formation. In the core experiments, the addition of primary silicates (olivine) drove solution δ^7Li to lower values, implying more congruent weathering. Further, the large effect of the exchangeable pool on Li in these experiments (>80%) contrasts to experiments where relatively fresh basalt was reacted with water with almost no initial pool of clay minerals (Pogge von Strandmann et al., 2019a). In those experiments, the exchangeable fraction only comprised 12–16% of the total Li, with the rest due to clay mineral neoformation. This difference highlights the long timescales required to precipitate significant amounts of secondary minerals. In other words, by importing pre-formed soils into the laboratory (rather than only fresh rocks), these soil core experiments have very different characteristics from experiments with olivine alone. The strong affinity of Li for exchangeable sites means that, while it provides important information on weathering on natural

timescales, on relatively short timescales (e.g., associated with enhanced weathering), ion exchange may mean that dissolution effects are harder to observe.

5.4 Comparison of Li and Mg isotopes

Overall, there is a negative co-variation between Δ^{26}Mg and Δ^{7}Li (Fig. 9). Hence, despite the decoupling of the behaviour of Li and Mg due to the difference in effect the exchangeable pool exerts, in terms of artificial addition of olivine, both isotope systems exhibit a similar response. What this means is that in these through-flow experiments, the experimental duration was not long enough for significant secondary mineral formation to occur. In contrast, secondary mineral formation did occur within this length of time in closed system experiments (Pogge von Strandmann et al., 2019a). If secondary mineral formation were to occur, it would be expected that it would be different in the olivine core compared to the control core, due to the addition of dissolved cations (Gíslason et al., 1996).

In terms of natural weathering, therefore, these experiments can shed some light on "incipient weathering", which in weathering studies represents the initial or very early part of the weathering reaction, although it has never been clear to what extent it encompasses sorption or secondary mineral formation (Navarre-Sitchler et al., 2015). Incipient weathering has been used to explain several different observations in Li isotope space (Kisakurek et al., 2004; Millot et al., 2010; Rudnick et al., 2004; Ryu et al., 2014), including driving the dissolved phase both isotopically heavy (Millot et al., 2010) and leaving the isotope ratios of soils virtually unaltered (Ryu et al., 2014). In the case of these experiments,

initial weathering of fresh material ('incipient weathering") clearly drives the dissolved load towards the composition of the primary weathering material, with fractionation by secondary minerals having minimal additional effect.

In terms of enhanced weathering, these experiments show that, while olivine dissolution (and hence CO_2 drawdown) will occur during the initial phases, the ultimate effect of enhancing weathering (i.e. including the increase in the formation of secondary weathering products) still largely remains unknown, and will require multi-year experiments to examine and quantify.

6. Conclusions

A well-characterised experiment in a soil core was used to assess the controls on lithium and magnesium isotope ratios during weathering. Olivine was added to the top of one core and compared to a control core without olivine

For both Mg and Li, the exchangeable pool of sorbed elements on mineral surfaces in the soil exerted a significant role on the effluent composition, retarding the transport of chemical signals down the core by around 17–20 days. Ion exchange occurred in response to changing pore-water chemistry and imposed an isotope fractionation on effluent waters at the base of the core. This will also result in a significant amount of time before effluent isotope ratios finally reach a full steady-state, when the retarded, fractionated signal finally breaks through.

Input of Mg to the effluent solution were largely from dissolution of carbonate plus dissolution of silicate in the olivine core, which drove the δ^{26}Mg of the olivine core towards higher (more olivine-like) values with time. Mg isotopes were thus largely controlled by the congruent dissolution of different lithologies,

modified in the short-term by isotopic fractionation associated with sorption onto the exchangeable fraction (of ~0.5‰, similar to natural studies). This observation supports the idea of using Mg isotopes as a lithological tracer, though interpretation of such Mg isotope signals will be complex on timescales where the exchangeable pool in the soil is adjusting to change.

The Li isotopic fractionation between the lowest part of the core's exchangeable pool and that in fluids in the core is ~18‰, and is 4‰ between the solution and the total core's concentration-weighted exchangeable fraction, similar to that observed in natural systems for exchangeable Li. Addition of olivine and its subsequent dissolution drove the solution δ^7Li lower (towards that of olivine) with time, showing that addition of primary silicate increases weathering congruency (at least on the timescale of a few months).

The use of these isotope systems in enhanced weathering situations does not necessarily add information that could not be accessed by trace element concentrations, at least when it comes to determining dissolution rates (and hence CO_2 drawdown rates). Both isotope systems have, however, revealed that the exchangeable pool significantly retards the transport of elements derived from the dissolution of added silicates, when those silicates are added to a pre-existing soil complex. Hence, using either isotope ratios or trace elements to examine and quantify enhanced weathering will be significantly complicated by the exchangeable pool, because any dissolution signal can take a significant amount of time to recognisably arrive at a monitoring station. This will then likely cause an initial underestimation of the added silicate dissolution rates and fluxes, unless the monitoring duration extends to the total equilibration time. In terms of natural weathering signals, the long averaging time for seawater

records means this process will not matter. However, for archives of less integrated processes (e.g. speleothems), this process may be important.

Acknowledgements

Isotope analyses and PPvS were funded by NERC advanced fellowship NE/I020571/2 and ERC Consolidator grant 682760 – CONTROLPASTCO2. PR and GMH acknowledge funding from the Oxford Martin School through the Oxford Geoengineering Programme, and from the Hay Family. Nicolas Boehm and Thomas Phelan (University of Oxford) are thanked for their help with experimental construction and sample collection, and Doug Hammond (USC) for discussion about data interpretation.

Declaration of interests

The authors declare that they have no known competing financial interests or personal relationships that could have appeared to influence the work reported in this paper.

References

Andrews, M.G., Taylor, J. L., 2019. Combating climate change through enhanced weathering of agricultural soils, Elements. Mineralogical Society of America, pp. 253–258.

Berner, R.A., 2003. The long-term carbon cycle, fossil fuels and atmospheric composition. Nature, 426(6964): 323-326.

Berner, R.A., Lasaga, A.C., Garrels, R.M., 1983. The Carbonate-Silicate Geochemical Cycle and Its Effect on Atmospheric Carbon-Dioxide over the Past 100 Million Years. American Journal of Science, 283(7): 641-683.

Bouchez, J., von Blanckenburg, F., Schuessler, J.A., 2013. Modeling novel stable isotope ratios in the weathering zone. American Journal of Science, 313.

Chapela Lara, M., Buss, H.L., Pogge von Strandmann, P.A.E., Schuessler, J.A., Moore, O.W., 2017. The influence of critical zone processes on the Mg isotope budget in a tropical, highly weathered andesitic catchment. Geochimica Et Cosmochimica Acta, 202: 77–100.

Clergue, C. et al., 2015. Influence of atmospheric deposits and secondary minerals on Li isotopes budget in a highly weathered catchment, Guadeloupe (Lesser Antilles). Chemical Geology, 414: 28–41.

Colbourn, G., Ridgwell, A., Lenton, T.M., 2015. The time scale of the silicate weathering negative feedback on atmospheric CO2. Global Biogeochemical Cycles, 29: 583–596.

Davidson, M.R., Dickson, B.L., 1986. A porous flow model for steady-state transport of radium in ground waters. Water Resources Research, 23: 34–44.

Dellinger, M. et al., 2015. Riverine Li isotope fractionation in the Amazon River basin controlled by the weathering regimes. Geochimica Et Cosmochimica Acta, 164: 71–93.

Ebelmen, J.J., 1845. Sur les produits de la décomposition des espèces minérales de la famille des silicates. Annales des Mines, 7: 3–66.

Elliott, T., Thomas, A., Jeffcoate, A., Niu, Y.L., 2006. Lithium isotope evidence for subduction-enriched mantle in the source of mid-ocean-ridge basalts. Nature, 443(7111): 565–568.

Foster, G.L., Pogge von Strandmann, P.A.E., Rae, J.W.B., 2010. The boron and magnesium isotopic composition of seawater. Geochemistry Geophysics Geosystems, 11: Q08015, doi:10.1029/2010GC003201.

Gíslason, S.R., Arnorsson, S., Armannsson, H., 1996. Chemical weathering of basalt in southwest Iceland: Effects of runoff, age of rocks and vegetative/glacial cover. American Journal of Science, 296(8): 837–907.

Gislason, S.R. et al., 2009. Direct evidence of the feedback between climate and weathering. Earth and Planetary Science Letters, 277(1-2): 213-222.

Godderis, Y. et al., 2013. Rates of consumption of atmospheric CO2 through the weathering of loess during the next 100 yr of climate change. Biogeosciences, 10: 135–148.

Gou, L.-F. et al., 2019. Li isotopes in the middle Yellow River: Seasonal variability, sources and fractionation. Geochimica Et Cosmochimica Acta, 248: 88–108.

Goudie, A.S., Viles, H.A., 2012. Weathering and the global carbon cycle: Geomorphological perspectives. Earth-Science Reviews, 113: 59–71.

Hangx, S.J.T., Spiers, C.J., 2009. Coastal spreading of olivine to control atmospheric CO2 concentrations: A critical analysis of viability. International Journal of Greenhouse Gas Control, 3(6): 757-767.

Hartmann, J. et al., 2013. Enhanced chemical weathering as a geoengineering strategy to reduce atmopsheric carbon dioxide, supply nutrients, and mitigate ocean acidification. Reviews of Geophysics, 51: 113–150.

Hindshaw, R.S. et al., 2019. Experimental constraints on Li isotope fractionation during clay formation. Geochimica Et Cosmochimica Acta, 250: 219–237.

Huang, K.J., Teng, F.Z., Elsenouy, A., Li, W.-Y., Bao, Z.Y., 2013. Magnesium isotopic variations in loess: Origins and implications. Earth and Planetary Science Letters, 374: 60–70.

Huh, Y., Chan, L.H., Chadwick, O.A., 2004. Behavior of lithium and its isotopes during weathering of Hawaiian basalt. Geochemistry Geophysics Geosystems, 5: art. no.-Q09002.

Huh, Y., Chan, L.H., Edmond, J.M., 2001. Lithium isotopes as a probe of weathering processes: Orinoco River. Earth and Planetary Science Letters, 194(1-2): 189–199.

Huh, Y., Chan, L.H., Zhang, L., Edmond, J.M., 1998. Lithium and its isotopes in major world rivers: Implications for weathering and the oceanic budget. Geochimica Et Cosmochimica Acta, 62(12): 2039–2051.

Johnson, T.M., DePaolo, D.J., 1997. Rapid exchange effects on isotope ratios in groundwater systems 1. Development of a transport-dissolution-exchange model. Water Resources Research, 33: 187–195.

Kisakürek, B., James, R.H., Harris, N.B.W., 2005. Li and δ^7Li in Himalayan rivers: Proxies for silicate weathering? Earth and Planetary Science Letters, 237(3-4): 387–401.

Kisakurek, B., Widdowson, M., James, R.H., 2004. Behaviour of Li isotopes during continental weathering: the Bidar laterite profile, India. Chemical Geology, 212(1-2): 27-44.

Koehler, P., Abrams, J.F., Voelker, C., Hauck, J., Wolf-Gladrow, D.A., 2013. Geoengineering impact of open ocean dissolution of olivine on atmospheric CO2, surface ocean pH and marine biology. Environmental Research Letters, 8(1).

Koehler, P., Hartmann, J., Wolf-Gladrow, D.A., 2010. Geoengineering potential of artificially enhanced silicate weathering of olivine. Proceedings of the National Academy of Sciences of the United States of America, 107(47): 20228-20233.

Krishnaswami, S., Graustein, W.C., Turekian, K.K., Dowd, J.F., 1982. Radium, Thorium and Radioactive Lead Isotopes in Groundwaters - Application to the Insitu Determination of Adsorption-Desorption Rate Constants and Retardation Factors. Water Resources Research, 18(6): 1663-1675.

Lai, Y.J., Pogge von Strandmann, P.A.E., Dohmen, R., Takazawa, E., Elliott, T., 2015. The influence of melt infiltration on the Li and Mg isotopic composition of the Horoman Peridotite Massif. Geochimica Et Cosmochimica Acta, 164: 318–332.

Lemarchand, E., Chabaux, F., Vigier, N., Millot, R., Pierret, M.C., 2010. Lithium isotope systematics in a forested granitic catchment (Strengbach, Vosges Mountains, France). Geochimica Et Cosmochimica Acta, 74: 4612-4628.

Li, W.-Y. et al., 2010. Heterogeneous magnesium isotopic composition of the upper continental crust. Geochimica Et Cosmochimica Acta, 74: 6867–6884.

Liu, X.-L., Rudnick, R.L., McDonough, W.F., Cummings, M.L., 2013. Influence of chemical weathering on the composition of the continental crust: Insights from Li and Nd isotopes in bauxite profiles developed on Columbia River Basalts. Geochimica Et Cosmochimica Acta, 115: 73–91.

Liu, X.-L., Teng, F.Z., Rudnick, R.L., McDonough, W.F., Cummings, M.L., 2014. Massive magnesium depletion and isotope fractionation in weathered basalts. Geochimica Et Cosmochimica Acta, 135: 336–349.

Liu, X.-M., Wanner, C., Rudnick, R.L., McDonough, W.F., 2015. Processes controlling δ7Li in rivers illuminated by study of streams and groundwaters draining basalts. Earth and Planetary Science Letters, 409: 212–224.

Maher, K., Chamberlain, C.P., 2014. Hydrologic Regulation of Chemical Weathering and the Geologic Carbon Cycle. Science, 343: 1502–1504.

Marschall, H.R. et al., 2017. The boron and lithium isotopic composition of mid-ocean ridge basalts and the mantle. Geochimica Et Cosmochimica Acta, 207: 102–128.

Millot, R., Girard, J.P., 2007. Lithium Isotope Fractionation during adsorption onto mineral surfaces, International meeting, Clays in natural & engineered barriers for radioactive waste confinement, Lille, Frace.

Millot, R., Vigier, N., Gaillardet, J., 2010. Behaviour of lithium and its isotopes during weathering in the Mackenzie Basin, Canada. Geochimica Et Cosmochimica Acta, 74: 3897–3912.

Misra, S., Froelich, P.N., 2012. Lithium Isotope History of Cenozoic Seawater: Changes in Silicate Weathering and Reverse Weathering. Science, 335: 818–823.

Moosdorf, N., Renforth, P., Hartmann, J., 2014. Carbon Dioxide Efficiency of Terrestrial Enhanced Weathering. Environmental Science & Technology, 48(9): 4809-4816.

Murphy, M.J. et al., 2019. Tracing silicate weathering processes in the permafrost-dominated Lena River watershed using lithium isotopes. Geochimica Et Cosmochimica Acta, 245: 154–171.

Navarre-Sitchler, A.K., Brantley, S.L., Rother, G., 2015. How Porosity Increases During Incipient Weathering of Crystalline Silicate Rocks. In: Steefel, C.I., Emmanuel, S., Anovitz, L.M. (Eds.), Pore-scale geochemical processes. Reviews in Mineralogy and Geochemistry.

Oelkers, E.H. et al., 2019. Using stable Mg isotope signatures to assess the fate of magnesium during the in situ mineralisation of CO2 and H2S at the CarbFix site in SW-Iceland. Geochimica Et Cosmochimica Acta, 245: 542–555.

Opfergelt, S. et al., 2014. Magnesium retention on the soil exchange complex controlling Mg isotope variations in soils, soil solutions and vegetation in volcanic soils, Iceland. Geochimica Et Cosmochimica Acta, 125: 110–130.

Opfergelt, S. et al., 2012. Mechanisms of magnesium isotope fractionation in volcanic soil weathering sequences, Guadeloupe. Earth and Planetary Science Letters, 341: 176-185.

Phan, T.T. et al., 2016. Factors controlling Li concentration and isotopic composition in formation waters and host rocks of Marcellus Shale, Appalachian Basin. Chemical Geology, 420: 162–179.

Pistiner, J.S., Henderson, G.M., 2003. Lithium-isotope fractionation during continental weathering processes. Earth and Planetary Science Letters, 214(1-2): 327-339.

Pogge von Strandmann, P.A.E., Burton, K.W., James, R.H., van Calsteren, P., Gislason, S.R., 2008. The influence of weathering processes on riverine magnesium isotopes in a basaltic terrain. Earth and Planetary Science Letters, 276: 187-197.

Pogge von Strandmann, P.A.E., Burton, K.W., James, R.H., van Calsteren, P., Gislason, S.R., 2010. Assessing the role of climate on uranium and lithium isotope behaviour in rivers draining a basaltic terrain. Chemical Geology, 270: 227–239.

Pogge von Strandmann, P.A.E. et al., 2006. Riverine behaviour of uranium and lithium isotopes in an actively glaciated basaltic terrain. Earth and Planetary Science Letters, 251: 134–147.

Pogge von Strandmann, P.A.E. et al., 2016. The effect of hydrothermal spring weathering processes and primary productivity on lithium isotopes: Lake Myvatn, Iceland. Chemical Geology, 445: 4–13.

Pogge von Strandmann, P.A.E. et al., 2017a. Global climate stabilisation by chemical weathering during the Hirnantian glaciation. Geochemical Perspective Letters, 3: 230–237.

Pogge von Strandmann, P.A.E. et al., 2011. Variations of Li and Mg isotope ratios in bulk chondrites and mantle xenoliths. Geochimica Et Cosmochimica Acta, 75: 5247–5268.

Pogge von Strandmann, P.A.E. et al., 2019a. Experimental determination of Li isotope behaviour during basalt weathering. Chemical Geology, 517: 34–43.

Pogge von Strandmann, P.A.E., Frings, P.J., Murphy, M.J., 2017b. Lithium isotope behaviour during weathering in the Ganges Alluvial Plain. Geochimica Et Cosmochimica Acta, 198: 17–31.

Pogge von Strandmann, P.A.E., Henderson, G.M., 2015. The Li isotope response to mountain uplift. Geology, 43(1): 67–70.

Pogge von Strandmann, P.A.E., Hendry, K.R., Hatton, J.E., Robinson, L.F., 2019b. The Response of Magnesium, Silicon, and Calcium Isotopes to Rapidly Uplifting and Weathering Terrains: South Island, New Zealand. Frontiers in Earth Science, 7(240).

Pogge von Strandmann, P.A.E., Kasemann, S.A., Wimpenny, J.B., 2020. Lithium ad Lithium Isotopes in Earth's Surface Cycles. Elements, 16: 253–258.

Pogge von Strandmann, P.A.E., Olsson, J., Luu, T.-H., Gislason, S.R., Burton, K.W., 2019c. Using Mg isotopes to estimate natural calcite compositions and precipitation rates during the 2010 Eyjafjallajökull eruption Frontiers in Earth Science, 7.

Pogge von Strandmann, P.A.E. et al., 2012. Lithium, magnesium and silicon isotope behaviour accompanying weathering in a basaltic soil and pore water profile in Iceland. Earth and Planetary Science Letters, 339–340: 11–23.

Pogge von Strandmann, P.A.E. et al., 2014. Chemical weathering processes in the Great Artesian Basin: Evidence from lithium and silicon isotopes. Earth and Planetary Science Letters, 406: 24–36.

Pogge von Strandmann, P.A.E. et al., 2017c. Lithium isotopes in speleothems: Temperature-controlled variation in silicate weathering during glacial cycles. Earth and Planetary Science Letters, 469: 64–74.

Porcelli, D., Swarzenski, P.W., 2003. The behavior of U- and Th-series nuclides in groundwater, Uranium-Series Geochemistry. Reviews in Mineralogy & Geochemistry, pp. 317-361.

Raymo, M.E., Ruddiman, W.F., Froelich, P.N., 1988. Influence of late Cenozoic mountain building on ocean geochemical cycles Geology, 16: 649-653.

Renforth, P., 2012. The potential of enhanced weathering in the UK. International Journal of Greenhouse Gas Control, 10: 229-243.

Renforth, P., Jenkins, B.G., Kruger, T., 2013. Engineering challenges of ocean liming. Energy, 60: 442-452.

Renforth, P., Pogge von Strandmann, P.A.E., Henderson, G.M., 2015. The dissolution of olivine added to soil: Implications for enhanced weathering. Applied Geochemistry, 61: 109–118.

Rudnick, R.L., Tomascak, P.B., Njo, H.B., Gardner, L.R., 2004. Extreme lithium isotopic fractionation during continental weathering revealed in saprolites from South Carolina. Chemical Geology, 212(1-2): 45-57.

Ryu, J.-S. et al., 2016. Experimental investigation of Mg isotope fractionation during mineral dissolution and clay formation. Chemical Geology, 445: 135–145.

Ryu, J.-S., Vigier, N., Lee, S.-W., Lee, K.-S., Chadwick, O.A., 2014. Variation of lithium isotope geochemistry during basalt weathering and secondary mineral transformations in Hawaii. Geochimica Et Cosmochimica Acta, 145: 103–115.

Saenger, C., Wang, Z., 2014. Magnesium isotope fractionation in biogenic and abiogenic carbonates: implications for paleoenvironmental proxies. Quaternary Science Reviews, 90: 1–21.

Sauzéat, L., Rudnick, R.L., Chauvel, C., Garcon, M., Tang, M., 2015. New perspectives on the Li isotopic composition of the upper continental crust and its weathering signature. Earth and Planetary Science Letters, 428: 181–192.

Schuiling, R.D., de Boer, P.L., 2010. Coastal spreading of olivine to control atmospheric CO2 concentrations: A critical analysis of viability. Comment: Nature and laboratory models are different. International Journal of Greenhouse Gas Control, 4(5): 855-856.

Schuiling, R.D., Krijgsman, P., 2006. Enhanced weathering: An effective and cheap tool to sequester CO2. Climatic Change, 74(1-3): 349-354.

Shalev, N. et al., 2018. Mg Isotope Inter-Laboratory Comparison of Reference Materials from Earth-Surface Low-Temperature Environments. Geostandards and Geoanalytical Research, in press.

Stallard, R.F., Edmond, J.M., 1983. Geochemistry of the Amazon .2. The Influence of Geology and Weathering Environment on the Dissolved-Load. Journal of Geophysical Research-Oceans and Atmospheres, 88(NC14): 9671-9688.

Stefansson, A., Gislason, S.R., 2001. Chemical weathering of basalts, Southwest Iceland: Effect of rock crystallinity and secondary minerals on chemical fluxes to the ocean. American Journal of Science, 301(6): 513-556.

Taylor, L.L. et al., 2020. Enhanced weathering strategies for stabilizing climate and averting ocean acidification. Nature Climate Change, 6: 402–406.

Teng, F.Z., Li, W.Y., Rudnick, R.L., Gardner, L.R., 2010. Contrasting lithium and magnesium isotope fractionation during continental weathering. Earth and Planetary Science Letters, 300: 63-71.

Teng, F.Z. et al., 2015. Interlaboratory comparison of magnesium isotopic compositions of 12 felsic to ultramafic igneous rock standards analyzed by MC-ICPMS. Geochemistry Geophysics Geosystems, 16.

Tessier, A., Campbell, P.G.C., Bisson, M., 1979. Sequential Extraction Procedure for the Speciation of Particulate Trace Metals. Analytical Chemistry, 51(7): 844-851.

Tipper, E.T., Gaillardet, J., Louvat, P., Capmas, F., White, A.F., 2010. Mg isotope constraints on soil pore-fluid chemistry: Evidence from Santa Cruz, California. Geochimica Et Cosmochimica Acta, 74: 3883-3896.

Tipper, E.T., Galy, A., Bickle, M., 2008. Calcium and magnesium isotope systematics in rivers draining the Himalaya-Tibetan-Plateau region:

Lithological or fractionation control? Geochimica Et Cosmochimica Acta, 72: 1057-1075.
Tipper, E.T., Galy, A., Bickle, M.J., 2006a. Riverine evidence for a fractionated reservoir of Ca and Mg on the continents: Implications for the oceanic Ca cycle. Earth and Planetary Science Letters, 247(3-4): 267-279.
Tipper, E.T. et al., 2006b. The magnesium isotope budget of the modern ocean: Constraints from riverine magnesium isotope ratios. Earth and Planetary Science Letters, 250(1-2): 241-253.
Tsai, P.-H., You, C.-F., Huang, K.-F., Chung, C.-H., Sun, Y.-B., 2014. Lithium distribution and isotopic fractionation during chemical weathering and soil formation in a loess profile. Journal of Asian Earth Sciences, 87: 1–10.
Vigier, N., Gislason, S.R., Burton, K.W., Millot, R., Mokadem, F., 2009. The relationship between riverine lithium isotope composition and silicate weathering rates in Iceland. Earth and Planetary Science Letters, 287(3-4): 434–441.
Walker, J.C.G., Hays, P.B., Kasting, J.F., 1981. A Negative Feedback Mechanism for the Long-Term Stabilization of Earths Surface-Temperature. Journal of Geophysical Research-Oceans and Atmospheres, 86(NC10): 9776-9782.
West, A.J., Galy, A., Bickle, M., 2005. Tectonic and climatic controls on silicate weathering. Earth and Planetary Science Letters, 235(1-2): 211–228.
White, A.F., Brantley, S.L., 2003. White, A.F., Brantley, S.L., 2003. The effect of time on the weathering of silicate minerals: why do weathering rates differ in the laboratory and field? Chemical Geology, 202: 479–506.
Wimpenny, J. et al., 2011. The behaviour of magnesium and its isotopes during glacial weathering in an ancient shield terrain in West Greenland. Earth and Planetary Science Letters, 304(1-2): 260-269.
Wimpenny, J., Colla, C.A., Yin, Q.Z., Rustad, J.R., Casey, W.H., 2014. Investigating the behaviour of Mg isotopes during the formation of clay minerals. Geochimica Et Cosmochimica Acta, 128: 178–194.
Wimpenny, J. et al., 2015. Lithium isotope fractionation during uptake by gibbsite. Geochimica Et Cosmochimica Acta, 168: 133–150.
Wimpenny, J. et al., 2010. Glacial effects on weathering processes: New insights from the elemental and lithium isotopic composition of West Greenland rivers Earth and Planetary Science Letters, 290: 427-437.

Figure 1. Schematic of the experimental setup. The plough layer depth was 0.2m (figure modified from Renforth et al., 2015).

Figure 2. A) Li isotope profiles for bulk soils and exchangeable leaches. B) Bulk soil, exchangeable and carbonate δ^{26}Mg with soil depth. Analytical uncertainty is smaller than the symbol sizes.

Figure 3. Effluent concentrations and isotope ratios. (A) Li concentrations; (B) Li isotope ratios, with the dashed line representing the composition of the olivine, and the shaded area the composition of the bulk soils. (C) Mg concentrations from Renforth et al. (2015); (D) Mg isotope ratios, with the dashed lines representing the composition of the added olivine and leached carbonate fractions, as labelled, while the shaded areas represent the bulk soils and exchangeable soil Mg fractions. The error bars represent the 2sd analytical uncertainty, unless smaller than the symbols.

Figure 4. Mg mass balance for the initial and final effluent solutions.

Figure 5. Li mass balance for the initial and final effluent solutions.

Figure 6. Mg isotopes as a function of the Mg/Ca ratio of the effluent solutions. The olivine core's effluent is clearly affected by a Mg-rich and isotopically heavy phase.

Figure 7. The Li concentration and isotope ratio of the exchangeable pool in the soil column.

Figure 8. A) Correlation between the Li isotope difference between the cores and the olivine dissolution rate (determined from Mg concentrations; Renforth et al., 2015). A logarithmic fit is shown because if the fit were linear, fractionation due to weathering could increase indefinitely. B) Relationship between the Mg

isotope difference between the drip waters from both cores and the olivine weathering rate determined from Mg concentrations. The error bars represent the 2sd propagated uncertainty.

Figure 9. The isotopic difference between the control and olivine cores for both Li and Mg isotopes plotted relative to each other.

Table 1. Li and Mg concentration and isotope ratios of the bulk soils, and their exchangeable and carbonate fractions (based on Na-acetate and acetic acid buffered with Na-acetate leaches, respectively).

Depth	Fraction	Li ng g^{-1}	δ^{7}Li ‰	2sd		
Initial olivine		1210	2.7	0.3		
0-10cm	Bulk soil	2050	-0.7	0.2		
	Exchangeable	11.0	6.6	0.4		
10-20cm	Bulk soil	2050	-0.5	0.2		
	Exchangeable	14.4	9.7	0.1		
20-30cm	Bulk soil	2150	-0.4	0.3		
	Exchangeable	14.5	10.2	0.7		
30-40cm	Bulk soil	3040	0.0	0.6		
	Exchangeable	12.3	12.6	0.2		
40-50cm	Bulk soil	2800	-0.3	0.2		
	Exchangeable	9.30	10.8	0.7		
50-60cm	Bulk soil	2640	0.7	0.1		
	Exchangeable	7.61	7.1	0.2		
60-70cm	Bulk soil	2100	0.6	0.3		
	Exchangeable	8.64	5.6	0.9		
70-80cm	Bulk soil	1000	0.7	0.1		
	Exchangeable	6.59	2.1	0.1		
80-90cm	Bulk soil	2860	2.1	0.1		
	Exchangeable	5.96	-5.9	0.1		
		Mg µg g^{-1}	δ^{25}Mg ‰	2sd	δ^{26}Mg ‰	2sd
Initial olivine		286,000	-0.12	0.01	-0.23	0.02
0-10cm	Bulk soil	3210	-0.31	0.03	-0.62	0.04
15-20cm	Exchangeable	30.0	-1.16	0.00	-2.18	0.02
	Carbonate	600	-1.71	0.07	-3.24	0.04

	Residue		-0.35	0.02	-0.71	0.05
	Bulk soil	3130	-0.35	0.01	-0.65	0.07
	Bulk soil rpt		-0.29	0.08	-0.59	0.06
45-50cm	Exchangeable	25.0	-0.88	0.06	-1.72	0.03
	Carbonate	269	-1.67	0.04	-3.27	0.04
	Bulk soil	3050	-0.27	0.02	-0.43	0.11
60-65cm	Bulk soil	3220	-0.14	0.03	-0.35	0.02
85-90cm	Exchangeable	8.54	-0.81	0.04	-1.54	0.08
	Carbonate	993	-1.73	0.04	-3.31	0.05
	Residue		-0.10	0.04	-0.17	0.04
	Bulk soil	3480	-0.15	0.07	-0.35	0.05
	Bulk soil rpt		-0.14	0.01	-0.33	0.03

Table 2. Li and Mg concentrations and isotope ratios of the effluent solutions.

Days	Li ng g^{-1}	δ^{7}Li ‰	2sd	Days	Mg µg g^{-1}	δ^{25}Mg ‰	2sd	δ^{26}Mg ‰	2sd
Control				**Control**					
5	1.2	12.4	0.1	5	5.97	-1.02	0.05	-1.94	0.04
10	1.0	10.9	0.1	10	6.79	-1.00	0.04	-1.91	0.07
15	0.9	10.8	0.5	17	6.79	-1.03	0.02	-1.94	0.01
20	1.0	11.5	0.4	19	5.96	-1.06	0.01	-2.00	0.09
25	1.0	19.7	0.4	45	3.30	-1.18	0.05	-2.30	0.06
30	1.1	17.6	0.3	56	2.55	-1.28	0.06	-2.42	0.07
35	1.1	20.0	0.1	65	3.06	-1.32	0.02	-2.48	0.05
45	1.2	21.6	0.5	91	2.27	-1.33	0.03	-2.52	0.04
54	1.3	24.2	0.5	107	1.76	-1.36	0.04	-2.62	0.03
89	1.3	22.3	0.3	117	1.75	-1.29	0.01	-2.52	0.03
101	1.2	20.2	0.5	129	2.27	-1.43	0.06	-2.73	0.08
113	1.2	20.2	0.7						
125	1.1	23.6	0.6						
133	1.1	23.4	0.6						
Olivine				**Olivine**					
5	1.2	13.3	0.4	5	7.03	-0.97	0.05	-1.86	0.04
10	1.1	12.9	0.1	10	8.36	-1.03	0.02	-1.95	0.09
15	1.2	12.5	0.5	17	7.49	-0.98	0.02	-1.86	0.07
20	1.0	11.9	0.1	19	7.63	-0.96	0.05	-1.80	0.02
25	1.2	12.5	0.5	45	5.99	-0.95	0.06	-1.86	0.04
30	1.3	14.1	0.2	56	7.29	-1.00	0.07	-1.90	0.02
35	1.3	15.3	0.2	65	6.35	-1.04	0.06	-1.97	0.08
45	1.3	14.7	0.4	91	6.41	-0.97	0.02	-1.80	0.08
54	1.3	14.0	0.6	107	4.69	-0.86	0.02	-1.73	0.06
89	1.4	15.6	0.1	117	5.49	-0.90	0.05	-1.81	0.03
101	1.3	12.2	0.5	129	4.63	-0.93	0.05	-1.74	0.06
113	1.3	14.9	0.3						
125	1.2	16.5	0.5						

133	1.2	16.6	0.9

Highlights

- Enhanced weathering experiments mimic geoengineering methods
- Crushed olivine is added to a soil core, and compared to a control core.
- Lithium and Magnesium isotopes are measured in solids and drip waters
- Both isotopes are strongly affected by retardation by the soil exchangeable complex